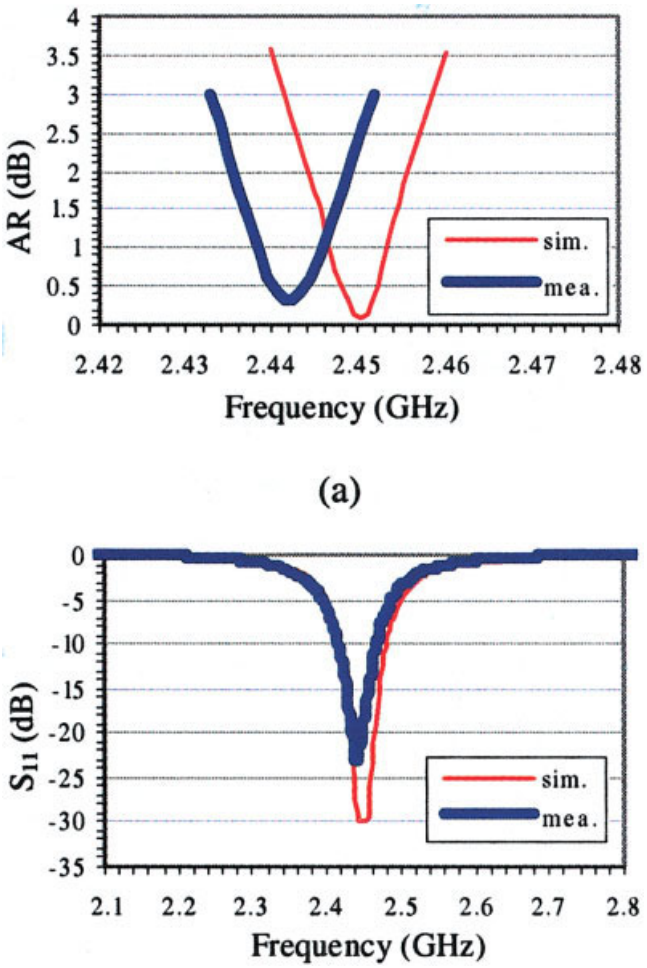

Figure 9 Results for (a) axial ratio and (b) return loss. [Color figure can be viewed in the online issue, which is available at www.interscience.wiley.com.]

$$\theta_m = \pi + \tan^{-1}\left(jZ_{0m}\frac{Z_{in} - Z_0}{Z_{0m}^2 - Z_{in}Z_0}\right). \tag{15b}$$

For this matching network, only a certain range of Z_{in} can be matched, as shown in Figure 8, and this determines the maximum value of the offset position x_0.

4. RESULTS

A nearly-square-patch antenna has been designed with an offset microstrip feed location at $0.35a$. From simulation, it was found that $Z_{in} = 93.8 - j64.3\Omega$, which was used to design the matching network. The parameters of the designed antenna operating at 2.45 GHz are summarized in Table 1.

Figure 9(a) shows a comparison of the simulated and measured results for the axial ratio of the designed antenna. The measured axial ratio was 0.34 dB at 2.442 GHz, which is less than a 0.5% shift from the design frequency.

Figure 9(b) shows that there is good agreement between the simulated and measured results for the return loss.

5. CONCLUSION

Based on the cavity model, simple linear equations have been derived and used to design a CP patch antenna. To obtain a compact form of the antenna, the design of a simple matching network has also been presented. The practical antenna shows good axial ratio and return loss and is in close agreement with the results predicted by the simulation.

ACKNOWLEDGMENTS

The authors would like to acknowledge the assistance of Peter Gale, Peter Elsdon, Stan Scott, and Prof. Z. Ghassemlooy.

REFERENCES

1. J.Q. Howell, Microstrip antennas, IEEE Trans Antennas Propagat AP-23 (1975), 90–93.
2. K.R. Carver and J.W. Mink, Microstrip antenna technology, IEEE Trans Antennas Propagat AP-29 (1981), 2–24.
3. M. Haneishi and Y. Suzuki, Circular polarisation and bandwidth, in Handbook of microstrip antennas, Chap. 4, J.R. James and P.S. Hall (Eds.), Peter Peregrinus Ltd., London, UK, 1989.
4. M.I. Aksun, S.L. Chuang, and Y.T. Lo, On slot-coupled microstrip antennas and their applications to CP operation: Theory and experiment, IEEE Trans Antennas Propagat 38 (1990), 1224–1230.
5. Y.T. Lo, B. Engst, and R.Q. Lee, Simple design formulas for circularly polarised microstrip antennas, IEE Proc Pt H 135 (1988), 213–215.
6. M. Haneishi and S. Yoshida, A design method of circularly polarized rectangular microstrip antenna by one-point feed, Electron Commun Jpn 64-B (1981), 46–54.
7. K.L. Wong, W.H. Hsu, and C.K. Wu, Single-feed circularly polarized microstrip antenna with a slit, Microwave Opt Technol Lett 18 (1998), 306–308.
8. J.L. Kerr, Microstrip polarization techniques, Proc 1978 Antenna Applic Symp, University of Illinois, Urbana, Allerton Park, IL, 1978.
9. E.G. Lim, Circular polarised microstrip antenna design using segmental methods, Ph.D. thesis, University of Northumbria at Newcastle, U.K., 2002.
10. Ansoft Ensemble v8, Ansoft Corporation, 2001.
11. M. Kirschning, R.H. Jansen, and N.H.L. Koster, Accurate model for open end effect of microstrip lines, Electron Lett 17 (1981), 123–125.
12. H.A. Atwater, Reflection coefficient transformations for phase-shift circuits, IEEE Trans Microwave Theory Tech MTT-28 (1980), 563–568.

ANALYSIS OF THICK-WIRE ANTENNAS USING A NOVEL AND SIMPLE KERNEL TREATMENT

F. D. Quesada Pereira, J. L. Gómez Tornero, D. Cañete Rebenaque, J. Pascual García, and A. Álvarez Melcón
Technical University of Cartagena
Campus Muralla del Mar s/n
30202 Cartagena
Murcia, Spain

Received 9 February 2005

ABSTRACT: *This paper presents novel aspects concerning the analysis of thick-wire antennas. The analysis is carried out using an integral equation (IE) technique, in which the kernel is treated with a novel numerical-integration procedure. A comparison with other techniques are included, showing the advantages of the newly proposed method. The novel treatment of the kernel requires the efficient extraction of the singularities. For this purpose, two different techniques are presented, and their advantages and drawbacks are discussed. Using the procedure proposed, complex thick wire antennas with rotational symmetry are analyzed. A combined antenna composed of cylindrical and conical sections is studied. The results show that the new techniques derived are efficient and lead to accurate results.* © 2005 Wiley Periodicals, Inc.

Microwave Opt Technol Lett 46: 410–417, 2005; Published online in Wiley InterScience (www.interscience.wiley.com). DOI 10.1002/mop.21002

Key words: *integral equations; wire antennas; numerical analysis; kernel singularity*

1. INTRODUCTION

The study of wire antennas has been extensively treated in the technical literature. For the analysis of wire antennas, the so-called thin-wire kernel has been extensively used in the past due to its efficiency [1]. The main limitation of this approach is that only electrically thin antennas can be treated ($a/\lambda < 0.01$). Due to this limitation, complex antennas composed of thick cylindrical and conical elements have always been studied using time-consuming techniques based on discretization of the entire metallic area [2].

To the authors' knowledge, only a few techniques have been developed to cope with thick-wire structures ($\lambda/a < 0.2$) [3, 4]. In that research, the exact series representation of the cylindrical wire kernel was used [3, 5]. While the technique is efficient, when thick-wire elements are to be studied, more terms in the Green's functions series must be included in order to maintain a reasonable degree of accuracy. This has a strong impact on the efficiency of the method. Also, the technique is only valid for straight-wire elements; it breaks down when curved wires are used. Finally, the technique derived in [3] has been applied only to very simple thick-wire dipoles of half and quarter wavelengths.

In this paper, we derive a more flexible technique for the treatment of thick-wire elements. This technique formulates a full Galerkin approach to the method of moments (MoM) solution for the cylindrical-wire problem. The kernel of the resulting integral equation (IE) is evaluated numerically in its full form. This is efficiently accomplished by using quadrature formulas, which are especially well suited for circular-integration paths [6]. The numerical results comparing this technique with the exact series approximation are included. The advantages of this new technique are stressed, particularly those related to the slow convergence of the exact series approximation close to the singularity.

Two different approaches are developed for the treatment of the kernel singularity. The first is based on the use of elliptic integrals. This kind of implementation has been chosen as a singularity-extraction technique in a number of papers published previously [7]. However, in this study, the procedure has been extended to cope with a more robust Galerkin MoM solution of the cylindrical antenna, using rooftop basis and testing functions. Alternatively, a novel singularity-extraction procedure is developed, based on a transformation from the canonical cylindrical-coordinate system to a new local polar plane, defined in the vicinity of the singularity. A comparison of the behavior exhibited by the two different numerical techniques has been performed, showing their validity.

The practical value of the derived approach is that it can be used for the analysis of complex thick-wire antennas exhibiting rotational symmetry, with a considerable reduction in the computational cost. In this paper, the technique is used to study a complex combined antenna composed of several cylindrical and conical elements. The results obtained with the new approach are compared with a standard surface IE based on a triangular discretization of the whole surface [2]. The results obtained with the new technique are accurate, and lead to a considerable reduction in the computational cost, as compared with the standard surface IE.

2. KERNEL CONSIDERATIONS FOR WIRE ANTENNAS

In the frame of the IE applied to wire antennas (Fig. 1), the key element to be considered in the formulation is the so-called kernel of the IE. If the currents are considered to be uniformly distributed about the circular surface of the wire, then it is demonstrated that the kernel can be cast in the following form:

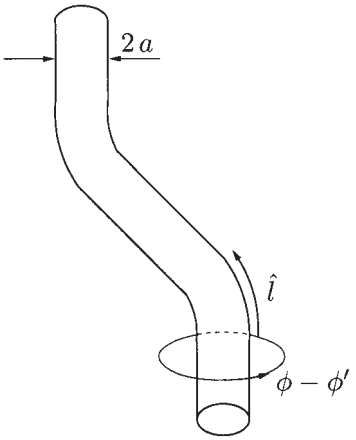

Figure 1 Cylindrical wire antenna with relevant geometrical parameters

$$K(l, l') = \frac{1}{4\pi^2} \int_0^{2\pi} \int_0^{2\pi} \frac{e^{-jk_0R}}{R} \, d\phi' d\phi. \tag{1}$$

If the cylindrical structure is rotationally symmetric, then the kernel can be further simplified. If it is assumed that the rotational symmetry axis is z, then the kernel can be written as

$$K(z, z') = \frac{1}{2\pi} \int_0^{2\pi} \frac{e^{-jk_0R}}{R} \, d(\phi - \phi'), \tag{2}$$

where the spatial distance R is defined as

$$R = \sqrt{(z - z')^2 + \rho^2 + a^2 - 2\rho a \cos(\phi - \phi')}. \tag{3}$$

In the above expression, a is the radius of the source segment and ρ is the radius of the observation segment. The previous expression has been written in closed form in [5] as follows:

$$K(z - z') = \frac{e^{-jk_0R}}{R} - j\beta \sum_{n=1}^{\infty} \frac{(k_0^2 \rho a)^{2n} (2n-1)!!}{(2n)!(2n)!!} \frac{h_{2n}^{(2)}(k_0 R)}{(k_0 R)^{2n}}, \tag{4}$$

where now the spatial distance reduces to: $R = \sqrt{(z - z')^2 + \rho^2 + a^2}$, and $h_\upsilon^{(2)}$ is the spherical Hankel function of the second kind and order υ.

We have found two main problems when using the closed-form expression for the kernel. The first is that convergence of the series can be very slow when the thickness of the wire increases. The second problem is that the analytical expression is only valid for straight wires. Therefore, the analysis of curved antennas has to be carried out with numerical integration of the cylindrical kernel, as given by Eq. (1). This last procedure has been chosen for the analysis of the wire structures of this paper, as it is more suitable for general CAD codes. Numerical integration with the azimuth coordinates is efficiently carried out with a quadrature rule for the circumferences presented in [6]. Special care must be taken when

evaluating the integrals for the singular situation (that is, when the base and test cells are the same). To treat this special case, two algorithms are developed in the next section.

In addition, if the radius of the wire is electrically short ($a < 0.01\lambda$), the exact kernel expansion can be reduced without lack of accuracy to the first term of Eq. (4), thus yielding

$$K(z - z') \simeq \frac{e^{-jk_0R}}{R}. \tag{5}$$

The thin-kernel form in Eq. (5) is employed in traditional electromagnetic codes for the analysis of thin-wire antennas, as in NEC [8]. In this paper we present, for the first time, a numerical analysis of complex thick-wire antennas, by means of the above rigorous kernel treatment.

3. SINGULARITY TREATMENT

As explained in the previous section, the azimuth variation of the kernel is rigorously taken into account through the numerical integration shown in Eq. (1). This integration can be efficiently evaluated using the quadrature rules for circumferences derived in [6]. However, special care must be taken in the singular case. Numerical integration will only converge if a proper singularity-extraction procedure is applied. We now present two techniques to efficiently preform this singularity extraction. The first technique, which is semi-analytical, is based on the use of elliptic integrals, as introduced in [3]. In this paper, we adapt this technique for a Galerkin solution of the IE, employing rooftop basis and testing functions. The second technique relies on numerical integration, and it can be considered as an extension of the singular treatment procedure presented in [9].

3.1 Singularity Extraction Based on Elliptic Integrals

This extraction mechanism is based on the elliptic integral expressions derived in [7], in the context of a point-matching MoM solution. In this work, we extend this technique to the more robust Galerkin implementation using linear rooftop basis and testing functions.

Following this technique, we will express the kernel in Eq. (1) in terms of complete elliptical functions of the first kind [10]. This function can be further expressed as the sum of a polynomic expansion and a logarithmic function [6]. The logarithmic function contains the singular behavior of the Green's functions, and can be integrated analytically. The rest of the polynomic expansion is regular (containing no singularities), and therefore it is integrated using standard quadrature rules.

When the domains of variation for the azimuth variables (ϕ, ϕ') are the same (the case of the singular situation), the general kernel form in Eq. (1) can always be simplified as in Eq. (2), where only one integration along the azimuth direction is required. The singularity in this expression can be extracted by summing and subtracting the term $1/R$:

$$K(z, z') = \frac{1}{2\pi}\left[\int_0^{2\pi} \frac{1}{R}\, d\phi' + \int_0^{2\pi} \frac{e^{-j\beta R} - 1}{R}\, d\phi'\right], \tag{6}$$

where R is defined as in Eq. (3). The second term in this last expression is not singular, and can be evaluated using quadrature rules. This first singular term is expressed in terms of the complete elliptical function:

$$\frac{1}{\pi}\int_0^{\pi} \frac{1}{R}\, d\phi' = \frac{1}{\pi}\frac{1}{\sqrt{\rho a}}\, kF\left(\frac{\pi}{2}, k\right), \quad 0 \le k < 1, \tag{7}$$

where the complete elliptical function of first kind is defined as

$$F\left(\frac{\pi}{2}, k\right) = \int_0^{\pi/2} \frac{d\phi}{\sqrt{1 - k^2\sin^2\phi}} \tag{8}$$

and k is a parameter defined as

$$k = \frac{2\sqrt{\rho a}}{\sqrt{(z - z')^2 + (\rho + a)^2}}. \tag{9}$$

The above function diverges when $k \to 1$ [6]. When applying the MoM, this situation can occur during the computation of the singular interactions, for which $\rho = a$ and $z = z'$. In these cases, the associated integrals cannot be directly evaluated. However, since integration in the azimuth variable has been performed in Eq. (7), the resulting singularity is of logarithmic type and can be integrated analytically. To proceed, we first use the polynomic expansion of the complete elliptic function [6]:

$$F\left(\frac{\pi}{2}, k\right) = [a_0 + a_1m + a_2m^2 + a_3m^3 + a_4m^4] - [b_0 + b_1m + b_2m^2 + b_3m^3 + b_4m^4]\ln(m) + |\varepsilon(k^2)|, \tag{10}$$

where we have defined $m = 1 - k^2$, and the absolute error of the expansion is said to be: $|\varepsilon(k^2)| < 2\ 10^{-8}$ [6]. Also, the a_i and b_i coefficients are given in [6]. Using the value of k in Eq. (9), the new parameter m becomes

$$m = \left.\frac{(z - z')^2 + (\rho - a)^2}{(z - z')^2 + (\rho + a)^2}\right|_{\rho=a} = \frac{(z - z')^2}{(z - z')^2 + 4a^2}. \tag{11}$$

From this last expression, we see that in a singular point $z = z'$, the parameter m goes to zero, thus compensating the singularity introduced by the logarithmic function. Therefore, the only singular term remaining in Eq. (10) is $[a_0 - b_0\ln(m)]$. To treat this singular term, we first use the following transformation:

$$[a_0 - b_0\ln(m)] = 0.5\ln\left(\frac{16}{m}\right) = 0.5\ln\left[\frac{16[(z - z')^2 + 4a^2]}{(z - z')^2}\right], \tag{12}$$

which is valid, since $a_0 = 0.5\ln(16)$ and $b_0 = 0.5$. Using this transformation, the singular term of the function to be integrated (7), can be expressed as

$$\frac{1}{\pi\sqrt{\rho a}}\, k\, \frac{1}{2}\ln\left[\frac{16[(z - z')^2 + 4a^2]}{(z - z')^2}\right] = \frac{1}{2\pi}\frac{1}{\sqrt{(z - z')^2 + 4a^2}}\ln\left[\frac{16[(z - z')^2 + 4a^2]}{(z - z')^2}\right]. \tag{13}$$

For convenience, we now define the following transformation:

$$\xi = \frac{\sqrt{(z - z')^2 + 4a^2}}{2a}, \tag{14}$$

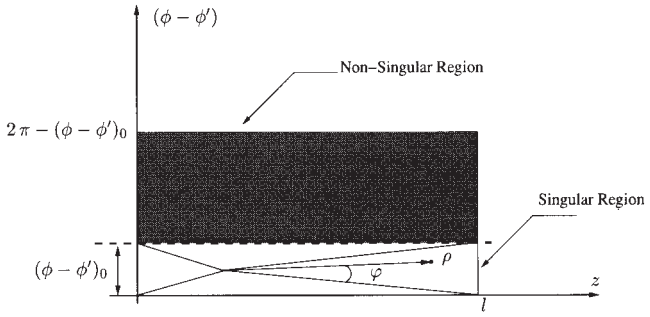

Figure 2 Integration space showing the singular and nonsingular regions. Integration in singular region is performed with polar coordinates (ρ, φ), as shown

which tends to one as the singularity approaches $z = z'$. Using this new transformation, we can rewrite Eq. (13) as

$$\frac{1}{2\pi}\frac{1}{2a}\left(1+\frac{1-\xi}{\xi}\right)\ln\left[\frac{16[(z-z')^2+4a^2]}{(z-z')^2}\right] = \frac{1}{2\pi}\frac{1}{2a}\left\{\ln\left[\frac{16[(z-z')^2+4a^2]}{(z-z')^2}\right] + \left(\frac{1-\xi}{\xi}\right)\ln\left[\frac{16[(z-z')^2+4a^2]}{(z-z')^2}\right]\right\}.$$

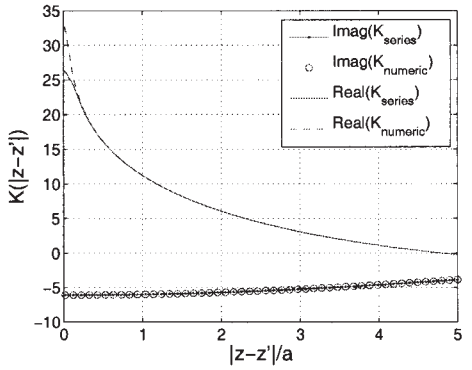

(a)

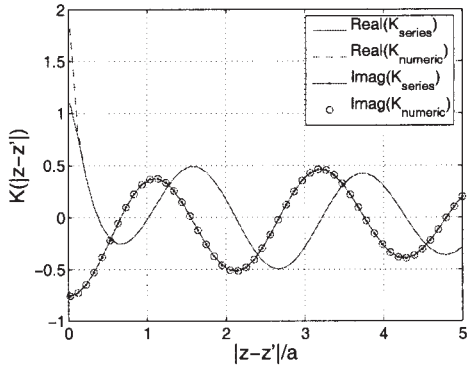

(b)

Figure 3 Comparison of the kernels K_{numeric} and K_{series} computed with Eqs. (1) and (4), respectively: (a) thin radius ($a/\lambda = 0.05$); (b) thick radius ($a/\lambda = 0.5$)

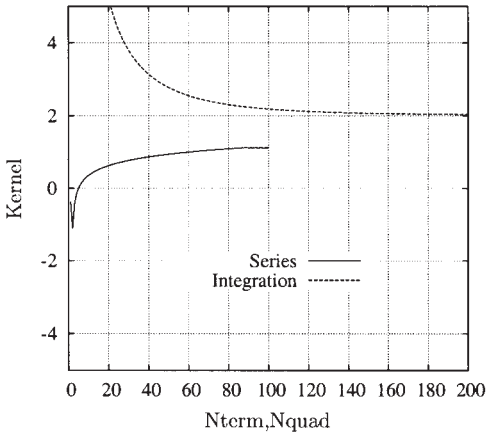

(a)

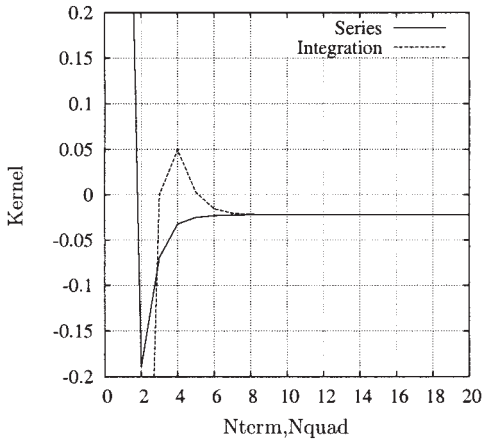

(b)

Figure 4 Convergence results obtained for a thick-wire antenna of radius $a/\lambda = 0.5$, close and far from the singularity (N_{term} = number of terms in the series; N_{quad} = number of integration points in quadrature): (a) close to singularity ($|z - z'| = a/50$); (b) far from singularity ($|z - z'| = a$)

The second term in this expression is not singular, since the singularity of the logarithm is compensated by the multiplying factor $(1 - \xi)/\xi$. The integral of the first singular term admits an analytical expression. If linear rooftop functions are selected in the MoM, the following analytical integral is used:

$$\int_0^l z'\ln\left[\frac{16[(z-z')^2+4a^2]}{(z-z')^2}\right]dz' = -\frac{1}{2}(z^2-l^2)\ln\left[\frac{16[(z-l)^2+4a^2]}{(z-l)^2}\right] + 2a^2\ln[(z-l)^2+4a^2] - 4za\tan^{-1}\left(\frac{z-l}{2a}\right) + \frac{1}{2}z^2\ln\left[\frac{16(z^2+4a^2)}{z^2}\right] + 2a^2\ln(z^2+4a^2) - 4za\tan^{-1}\left(\frac{z}{2a}\right), \quad (15)$$

where l is the length of the rooftop. For the electric scalar potential, the linear rooftop function becomes a constant charge inside the relevant cell. In this case, the following analytical integral is used:

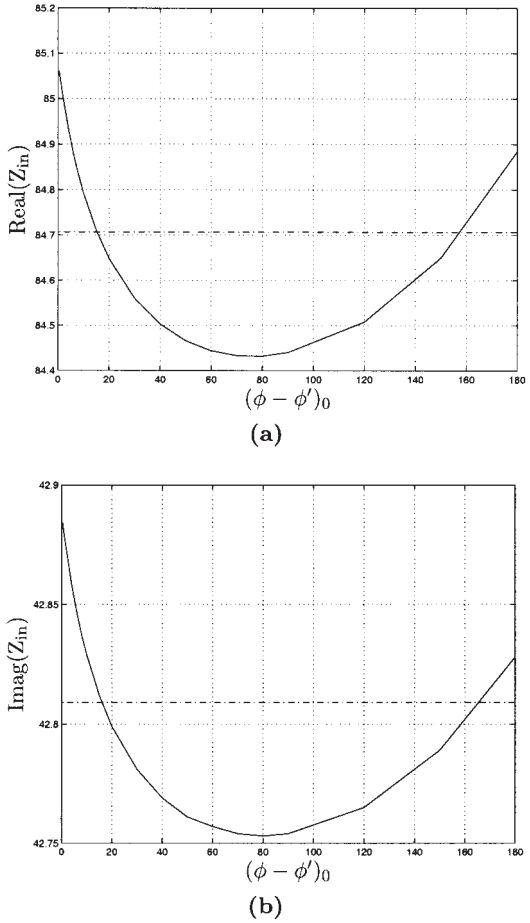

Figure 5 Input impedance obtained using the polar-integration technique as a function of the value of the critical angle, for a thin-wire dipole of radius $a/\lambda = 0.001$ (dashed line shows results obtained with the elliptic integral method; length of the dipole $L/\lambda = 0.5$): (a) real part; (b) imaginary part

$$\int_0^l \ln\left[\frac{16[(z-z')^2+4a^2]}{(z-z')^2}\right]dz' = -(z-l)\ln\left[\frac{16[(z-l)^2+4a^2]}{(z-l)^2}\right] - 4a\tan^{-1}\left[\frac{(z-l)}{2a}\right] + z\ln\left[\frac{16(z^2+4a^2)}{z^2}\right] + 4a\tan^{-1}\left(\frac{z}{2a}\right),$$

where, again, l is the length of the cell.

3.2 Singularity Extraction Based on Numerical Integration

To avoid the analytical complexities of the previous method, in this section we derive an alternative technique based on numerical integration. We will see that with this technique we gain simplicity without loss of accuracy.

To start, we first note that in the singular case the radii of the source and observer cells are equal, since both cells collapse to the same $a = \rho$. Under this condition, the distance in Eq. (3) can be simplified to

$$R = \sqrt{4a^2\sin^2\left(\frac{\phi-\phi'}{2}\right) + (z-z')^2}. \tag{16}$$

In the singularity, when $(\phi - \phi') \to 0$, the sine function can be approximated with the argument ($\sin x \simeq x$), resulting in the following equation:

$$R \simeq \sqrt{a^2(\phi-\phi')^2 + (z-z')^2}. \tag{17}$$

Then the strategy is to divide the whole integration domain along the azimuth direction, into singular and nonsingular regions (see Fig. 2). An azimuth critical value $[(\phi - \phi')_0]$ is chosen to separate both regions, as illustrated in Figure 2. In the singular region, the approximation of the sine function with its argument would be valid without loss of accuracy. Therefore, Eq. (17) can be used, and the singularity can be removed via integration with the polar coordinates. The Jacobean of the polar transformation exactly compensates the singularity of the kernel [9]. The radial variable of integration shown in Figure 2 can be expressed, from Eq. (17), as

$$\rho/a = \sqrt{(\phi-\phi')^2 + (z-z')^2}, \tag{18}$$

where, as can be seen, a scaling factor equal to the radius of the cell a needs to be applied. In the nonsingular region (the dark area in Fig. 2), the singularity is not present and, therefore, the integration can proceed using standard quadrature rules. It is worth noting that the argument to the sine function in Eq. (16) depends only on the integration variable $(\phi - \phi')$. Since the range of variation is always the same (from 0 to 2π), a fixed optimum value for the critical angle $[(\phi - \phi')_0]$ can be selected independently of the other geometrical parameters. We have found that a value of $[(\phi - \phi')_0] = 15°$ is optimum, and leads to relative errors in the evaluation of the input impedance of wire antennas lower than 0.1%.

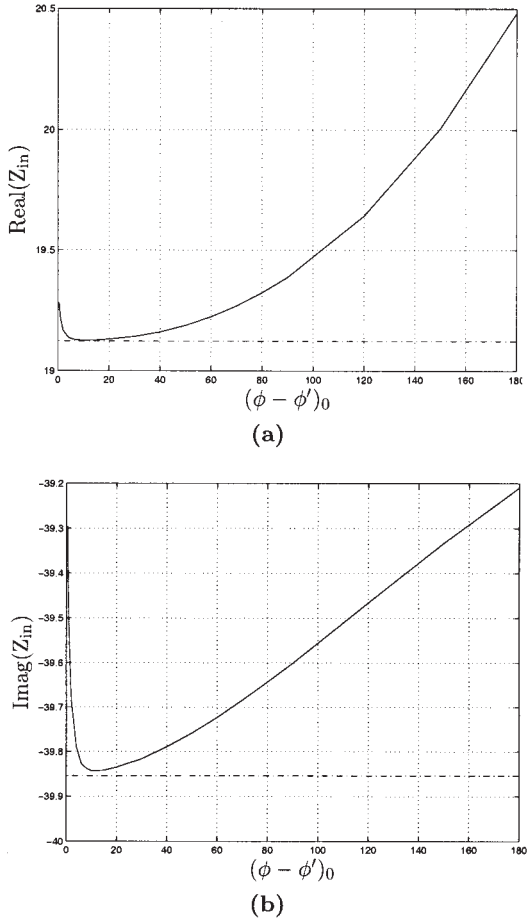

Figure 6 Similar results as in Fig. 5, but for a thick dipole of radius $a/\lambda = 0.1129$ and length $L/\lambda = 0.25$: (a) real part; (b) imaginary part

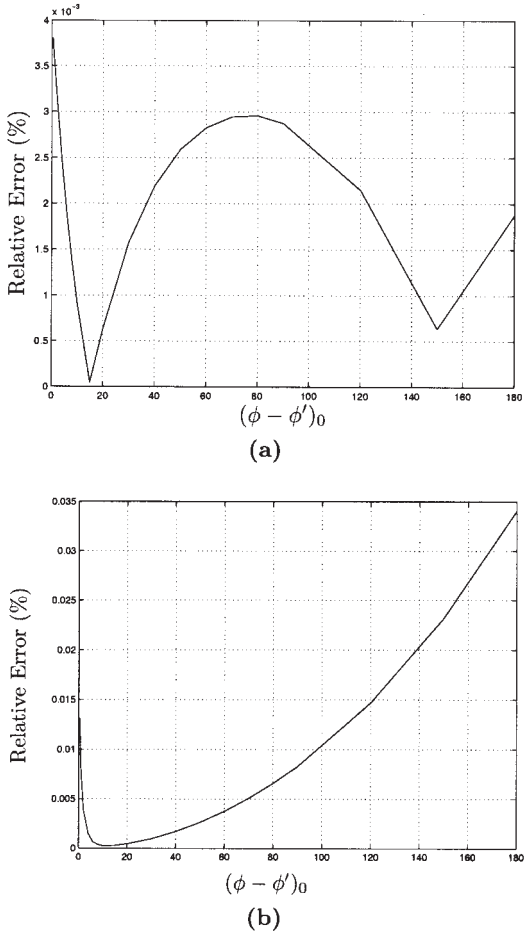

Figure 7 Relative errors for the input impedance obtained using the polar-integration technique with respect to the elliptic integral method (the error is minimum for an optimum value $(\phi - \phi')_0 \approx 15°$): (a) thin dipole ($a/\lambda = 0.001$); (b) thick dipole ($a/\lambda = 0.1129$)

4. RESULTS

Before applying the new techniques to the analysis of practical antennas, we are going to study how the proposed integration of the kernel behaves, as in Eq. (1), compared to the exact series expansion of Eq. (4). In Figure 3, we present the kernel computed with both approaches, for two different antenna radii ($a/\lambda = 0.05$, 0.5). We can see that the agreement between the two techniques is very good, even for the large-wire radii. The problems appear when the kernel is computed close to the singularity, relative to the wire radius. This effect is shown in Figure 3 for small values of source-observer distance (small $|z - z'|$ in Fig. 3). The differences in both results are due to a slow convergence of the exact series representation. This can be corrected, in principle, by adding more terms in the series. However, the problem when using this formulation is that numerical overflows easily occur when a sufficient number of terms in the series are included. This is due to the factorials appearing in the mathematical expression, which can easily expand for large values of n in Eq. (4). On the contrary, more integration points can be used in Eq. (1), with no limit, in order to have a correct representation of the kernel, and thus avoid losing accuracy. To illustrate the impact that these parameters have in the kernel calculation, Figure 4 shows the convergence obtained with both formulations, for two different source-observer separations ($|z - z'| = a/50$, a). When the separation is big, convergence is attained quickly with both techniques. However, close to the singularity, the convergence rate considerably decreases, as shown in Figure 4(a). Moreover, the correct result with the series representation cannot be obtained, since an overflow occurs when the number of terms is greater than 100. On the contrary, the numerical integration of the kernel reaches convergence with a quadrature rule of order 150. In these figures, only the convergence of the real part is shown, since the imaginary part converges very quickly in both cases and does not add any new information.

In the previous results, we have shown the difficulties associated with singularity in the cylindrical-wire kernel. When the source and observation cells are the same, other techniques, which are able to extract singularity, must be used. In this paper, we have presented two such techniques. In order to validate the singularity-extraction mechanisms introduced, we have compared the results for the input impedance of a dipole antenna, using the two techniques described in section 3. Figure 5 shows the real and imaginary parts of the input impedance obtained for a half-wavelength thin dipole of radius $a = 0.001\lambda$. The thick line shows the results obtained when the polar integration technique is applied, as a function of the value chosen for the critical angle: $[(\phi - \phi')_0]$. The dashed line shows the constant results obtained using the com-

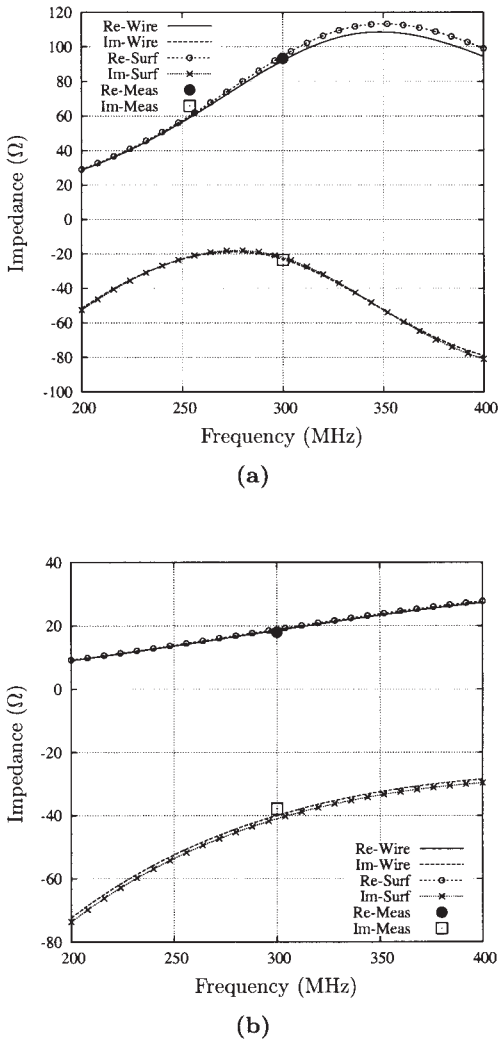

Figure 8 Input impedance for the two thick-wire dipoles presented in [3], comparing the thick-wire model and surface IE are compared (measured results at 300 MHz are also included): (a) length $L/\lambda = 0.5$, radius $a/\lambda = 0.0509$; (b) length $L/\lambda = 0.25$, radius $a/\lambda = 0.1129$

plete-elliptic integral technique. Similar results are presented in Figure 6, but for a thick dipole of radius $a = 0.113\lambda$. It can be seen that in both cases an optimum value around $[(\phi - \phi')_0] = 15°$ is observed, irrespective of the radius of the antenna. When this optimum value is used in the polar-integration technique, the results obtained are very similar to those obtained with using complete-elliptic integral. This behavior was expected, as discussed in subsection 3.2, and is related to the approximation of a sine function with its argument. In Figure 7, we present the relative errors obtained using the polar-integration technique, again as a function of the critical angle. It can be seen that, close to the optimum critical angle, relative errors lower that 0.1% are obtained for the input impedance.

As a further validation of the rigorous treatment of the kernel presented in section 2, together with the singularity-extraction mechanisms, we have calculated the input impedance of two thick dipoles presented in [3]. Figure 8 compares the results obtained from the measurements and the simulated data, computed using a standard surface IE employing triangular cells for the discretization [2]. For the wire model, only $N = 20$ segments have been used for the discretization, corresponding to 19 basis functions, while for the surface model, the geometry is discretized using 358 triangular cells corresponding to 527 basis functions. The agreement obtained is very good, but with the new thick-wire model, the overall numerical problem has been considerably reduced. The measured results presented in [3] at 0.3 GHz are also included, confirming the validity of the model.

The previous results indicate that the thick-wire model derived in this paper can be used to analyze more complex antenna geometries composed of arbitrary cylindrical and conical sections. Following this idea, we consider now a dual-band dipole antenna formed by four different cylindrical and conical sections, as shown in Figure 9. The antenna acts as two different dipoles, with each one operating in a different frequency band. The cylindrical sections are modeled as straight thick-wire elements, while the conical sections are modeled using a corresponding staircase approximation of the cone shape. To do this approximation, the conical section is divided in several linear cells. The radii are then varied from cell to cell in order to end up with the staircase approximation of the conical shape, as shown in Figure 9(b). The same structure

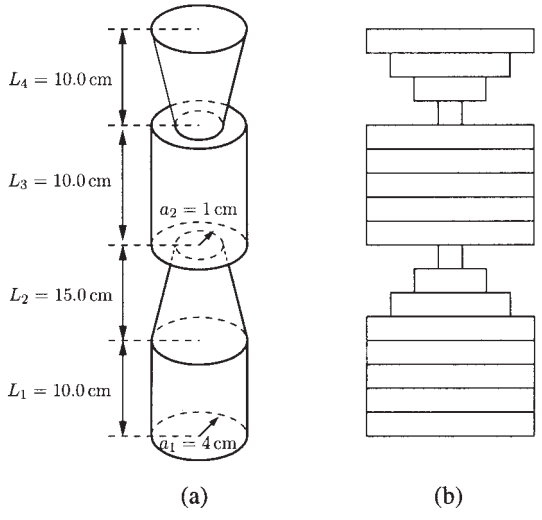

Figure 9 (a) Combined antenna for dual-band operation and (b) thick-wire model of the antenna

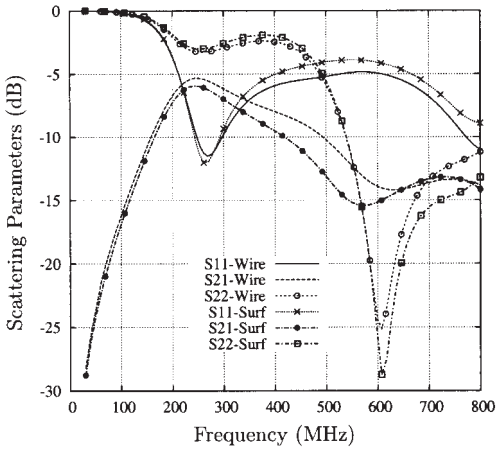

Figure 10 Scattering parameters for the two radiating dipoles of the combined antenna, comparing the thick-wire model and surface IE

is also analyzed using a standard surface IE by discretizing the whole metallic surface of Figure 9(a) with triangular cells. The novel thick-wire model employs $N = 10$ segments for each of the four sections, corresponding to a total of 39 basis functions. On the other hand, the full-surface IE is solved employing 874 triangular cells corresponding to a total of 1291 basis functions. The complete scattering parameters of the antenna are presented in Figure 10, including the coupling between the two sections. It can be seen that, again, good agreement is obtained between the two models, but with an important reduction of the global numerical burden when the thick-wire technique is used. We have seen that the results for the thick-wire model presented agree very well for cylindrical antennas with radius up to $a/\lambda = 0.1$. This demonstrates the usefulness of the new techniques derived in this paper, even for complex antenna geometries. To the authors' knowledge, this is the first time that a wire model has been used for the analysis and design of such complex antennas.

5. CONCLUSION

In this paper, we have presented several novel techniques for the accurate modeling of thick-wire antennas. We have demonstrated that by combining a rigorous integration of the cylindrical kernel, together with a suitable technique to extract the kernel singularities, very complex antennas exhibiting rotational symmetry can be analyzed. This technique considerably reduces the computational cost required for the analysis of complex thick-wire antennas, as compared with a standard surface IE. The results for an antenna containing cylindrical and conical elements have been presented. They demonstrate the accuracy of the method, together with the reduction of the computational cost.

REFERENCES

1. C.M. Butler and D.R. Wilton, Analysis of various numerical techniques applied to thin wire scatterers, IEEE Trans Antennas Propagat 23 (1975), 534–540.
2. S.M. Rao, D.R. Wilton, and A.W. Glisson, Electromagnetic scattering by surfaces of arbitrarily shape, IEEE Trans Antennas Propagat 30 (1982), 409–418.
3. D.H. Werner, A method of moments approach for the efficient and accurate modeling of moderately thick cylindrical wire antennas, IEEE Trans Antennas Propagat 46 (1998), 373–382.
4. A. Heldring and J.M. Rius, Efficient full-kernel evaluation for thin wire analysis, Microwave Opt Technol Lett 44 (2005), 477–480.

5. W.-X. Wang, The exact kernel for cylindrical antenna, IEEE Trans Antennas Propagat 39 (1991), 434–435.
6. M. Abramowitz and I.A. Stegun, Handbook of mathematical functions, Dover Publications, New York, 1972.
7. W.A. Davis, Numerical methods for wire structures, Tech Rpt, Virginia Polytechnic Institute and State University, 1995.
8. G.J. Burke and A.J. Poggio, Numerical electromagnetic code (NEC), method of moments, part II: Program description code, Tech Rpt, N00014-71-C-0187, Lawrence Livermore Laboratory, Livermore, CA, 1981.
9. F.Q. Pereira, J.L. Gómez Tornero, D.C. Rebenaque, J.P. García, and A.A. Melcón, Analysis of finite microstrip structures using an efficient implementation of the integral equation technique, Radio Sci 2004rs003036 (2005).
10. W.H. Press, S.A. Teukolsky, W.T. Vetterling, and B.P. Flannery, Numerical recipes in Fortran 90: The art of parallel scientific computing, Cambridge University Press, Cambridge, 1996.